

Derivation, Properties, and Simulation of a Gas-Kinetic-Based, Non-Local Traffic Model

Martin Treiber, Ansgar Hennecke, and Dirk Helbing

II. Institute of Theoretical Physics, University of Stuttgart, Pfaffenwaldring 57, D-70550 Stuttgart, Germany
(November 26, 2024)

We derive macroscopic traffic equations from specific gas-kinetic equations, dropping some of the assumptions and approximations made in previous papers. The resulting partial differential equations for the vehicle density and average velocity contain a non-local interaction term which is very favorable for a fast and robust numerical integration, so that several thousand freeway kilometers can be simulated in real-time. The model parameters can be easily calibrated by means of empirical data. They are directly related to the quantities characterizing individual driver-vehicle behavior, and their optimal values have the expected order of magnitude. Therefore, they allow to investigate the influences of varying street and weather conditions or freeway control measures. Simulation results for realistic model parameters are in good agreement with the diverse non-linear dynamical phenomena observed in freeway traffic.

05.70.Fh,05.60.+w,47.55.-t,89.40.+k

I. INTRODUCTION

Recently, traffic dynamics has become interesting to a rapidly growing community of physicists. This is not only due to its practical implications for optimizing freeway traffic, but even more because of the observed non-equilibrium phase transitions [1,2] and non-linear dynamical phenomena like the formation of traffic jams [3,4], stop-and-go traffic [5], and synchronized traffic [1,6]. It seems that all forms of congested traffic have almost universal properties which are largely independent of the initial conditions and the spatially averaged density, like the characteristic outflow from traffic jams of about 1800 ± 200 vehicles per kilometer and lane or their typical dissolution velocity of about -15 ± 5 kilometers per hour [7]. This universality arises from the highly correlated state of motion produced by traffic congestions [8,9].

Whereas classical approaches focussed on reproducing the empirically observed flow-density relation and the regime of unstable traffic flow, recent publications pointed out that it is more important to have traffic models which are able to describe the observed spectrum of non-linear phenomena and their characteristic properties [3,5,7,10]. We think that it would be desirable to develop models that are consistent with both aspects of empirical data. Such models have been proposed lately, including cellular automata models [11,9] and “microscopic” models of driver-vehicle behavior [12,13], and the macroscopic model discussed in this paper.

In order to have meaningful and measurable model parameters, we will relate our macroscopic model of freeway traffic to a “microscopic” model of driver vehicle behavior via a gas-kinetic derivation (cf. Sec. II). Derivations of this kind have been already proposed in a number of previous publications [14–17], but the correct treatment of the most interesting regime of moderate and high densities remained a problem. In [18–20], the effect of vehicular space requirements has been taken into account by a correlation factor reflecting the increased interaction

rate of vehicles (which can now be derived from simple and plausible arguments, cf. Sec. II B). In deriving the associated macroscopic equations, different approximations have been suggested, the most harmless of which was a gradient expansion [18,21]. This led to a viscosity term and some unexpected but essential high-density corrections containing spatial derivatives of different orders. However, the resulting partial differential equations were not very suitable for numerical simulations.

Meanwhile we managed to evaluate the Boltzmann-like gas-kinetic interaction term exactly (cf. Sec. II B). Since it turned out that a dynamical variance equation [4,22] is not necessary for a description of the presently known properties of traffic flows, we replaced it by a constitutive relation which—corresponding to a quasi-adiabatic approximation—agrees with the equilibrium variance. The resulting macroscopic traffic equations are coupled non-linear partial differential equations which can be represented in form of flux equations with a non-local and anisotropic source term [23]. For this reason, we can now apply various standard methods for numerical integration. It turns out that the non-local term has similar smoothing properties like a viscosity term, but it does not change the hyperbolic character of the partial differential equations to a parabolic one, and it has more favorable properties with respect to numerical stability. For this reason, our model allows a robust real-time simulation of freeway stretches up to several thousand kilometers on a usual PC.

Compared to previous macroscopic traffic models, the gas-kinetic-based traffic model (GKT model) proposed in the following takes into account the variance of vehicle velocities, which is basically proportional to the square of average velocity (cf. Eq. (21)), but with a density-dependent prefactor that determines the exact form of the flow-density relation in equilibrium. Moreover, the “optimal velocity” or “dynamical equilibrium velocity” \tilde{V}_e (cf. Eq. (31)), towards which the average velocity relaxes, depends not only on the local density, but

also on the average velocity, and, even more important, on the density and average velocity at an “interaction point” which is advanced by about the safe distance. Nevertheless, the equations are structurally related to, for example, the Kerner-Konhäuser model [3], so that we find many similar non-linear phenomena. This includes the sequence of stable, linearly unstable, and metastable regimes [5,24], the local breakdown effect [25], the local cluster effect [5], and the formation of dipole layers [24] at sufficiently large densities. We also obtain that, in the unstable traffic regime, the resulting flow-density relation differs from the equilibrium one (lying below the latter, cf. Fig. 9). In addition, we find that the outflow from traffic jams is independent of the initial conditions and the spatially averaged density (cf. Fig. 5). Moreover, the dissolution velocity of traffic jams varies only a little with density (cf. Fig. 7). Finally, the gas-kinetic-based model is able to explain the common phenomenon of synchronized congested traffic [26], if the inflow at on-ramps is taken into account.

It turns out that our model can be easily calibrated to the static and dynamic properties of traffic flow data by a certain systematic procedure (cf. Sec. III D). All parameters have a clear interpretation, since they are related to quantities characterizing the driver vehicle units like desired velocities or vehicle lengths (cf. Table I). At least some of the quantities like the typical desired velocity or the average time headway are directly measurable. Moreover, the optimal parameters obtained from a calibration to empirical data have the expected order of magnitude (cf. Table I). Therefore, the model allows to investigate the effect of speed limits, of a larger percentage of trucks, of bad weather conditions, etc. It will usually be sufficient to change the affected parameter values accordingly, instead of calibrating or even modifying the whole model for every new situation.

II. THE MODEL

A. Underlying Gaskinetic Equation

Similar to the gas-kinetic derivation of macroscopic equations for fluids, we start by formulating a kinetic equation for the locally averaged dynamics of driver-vehicles units, which play the role of the molecules, here. The kinetic equation describes the evolution of the coarse-grained phase-space density

$$\begin{aligned} \tilde{\rho}(x, v, t) = & \sum_{\alpha} \int dt' \int dx' \int dv' g(t-t', x-x', v-v') \\ & \times \delta(x' - x_{\alpha}(t)) \delta(v' - v_{\alpha}(t)), \end{aligned} \quad (1)$$

denoting the probability density of finding, at a given time t , a vehicle α at position x_{α} with velocity v_{α} . In more intuitive terms, $\tilde{\rho}$ corresponds to the spatial density of vehicles per lane times their velocity distribution. Since the GKT model is an effectively one-lane

model where lane changes and overtaking are only implicitly taken into account, there is no lane index. The coarse graining is performed by taking local averages over a weighting function $g(t-t', x-x', v-v')$ satisfying $\int dt' \int dx' \int dv' g(t-t', x-x', v-v') = 1$, which is localized in a microscopically large and macroscopically small neighborhood around x and in suitable neighborhoods around t and v . The particular choice of g is not relevant for the *form* of the macroscopic equations [27]. However, the scales Δt , Δx , and Δv are meaningful in that they enter the effective relations for the higher velocity moments like the variance.

The information specific to vehicular traffic is contained in the “microscopic” dynamics of individual driver-vehicle units. In the GKT model, we assume the vehicular dynamics of the form [13,28]

$$\begin{aligned} \frac{dx_{\alpha}}{dt} &= v_{\alpha}, \\ \frac{dv_{\alpha}}{dt} &= \frac{v_{\alpha}^0 - v_{\alpha}}{\tau_{\alpha}} - \sum_{\beta \neq \alpha} f_{\alpha\beta}. \end{aligned} \quad (2)$$

The first term on the right-hand side of Eq. (3) represents the acceleration of the driver-vehicle unit α to the desired velocity v_{α}^0 with an adaptation time of τ_{α} . On empty roads, this is the only acceleration term. Notice that v_{α}^0 is an intrinsic property of the driver-vehicle unit. The second term on the right-hand side of Eq. (3) represents the braking interaction of vehicle α due to slower vehicles β in front. It depends mainly on the subjective minimum safe time headway T_{α} to the car in front that driver α wants to keep. The details of the braking interaction will be discussed below.

In general, the parameters v_{α}^0 , τ_{α} , and the parameters of the braking interaction like T_{α} are different for each individual vehicle α . This could be respected by generalizing $\tilde{\rho}$ to a multi-dimensional phase-space density in a phase space spanned by the dimensions x , v , τ , v^0 , etc. This density would express the probability of finding at x a driver-vehicle unit with velocity v , whose microscopic parameters are τ , v^0 , etc. Paveri-Fontana applied this concept to the extra variable v^0 alone, formulating an equation for $\hat{\rho}(x, v, v^0, t)$ [15], which was further investigated by Helbing [17] and Wagner *et al.* [19].

In the GKT model, however, we assume that all deviations of the individual driving behavior from that of the “average driver” eventually lead to fluctuations of the velocity. For a nearly empty road this is obvious. Then, the braking term is negligible, and the distribution of vehicle velocities must converge to that of their desired velocities. In dense traffic, there are additional sources of velocity fluctuations. The time when vehicle α starts to brake in response to a slower vehicle in front depends on the individual safe time headway T_{α} . Obviously, driver α brakes later for lower values of T_{α} . Thus, different T_{α} lead to different velocities, even if *all* other parameters of the vehicles (in particular the desired velocities)

and all initial conditions are unchanged. In addition, imperfect driving behavior such as delayed acceleration or overbraking (i.e., braking more than necessary in a given situation) contributes to the velocity fluctuations [18].

If we are not interested in microscopic details, such fluctuations can be described in a global way by a fluctuating force in the acceleration equation (3), in analogy to hydrodynamic fluctuations [29]. Thus, we approximate Eq. (3) by

$$\frac{dv_\alpha}{dt} = \frac{V_0 - v_\alpha}{\tau} - \sum_{\beta \neq \alpha} \bar{f}_{\alpha\beta} + \xi_\alpha(t), \quad (4)$$

where $V_0 = \langle v_\alpha^0 \rangle := \frac{1}{N} \sum_\alpha v_\alpha^0$ and $1/\tau = \langle 1/\tau_\alpha \rangle$ are the averaged microscopic parameters of the acceleration term (N denotes the total number of vehicles). The braking term $\bar{f}_{\alpha\beta}$ is formulated with averaged parameters like $T = \langle T_\alpha \rangle$ as well. The fluctuating forces $\xi_\alpha(t)$ obey

$$\langle \xi_\alpha(t) \rangle = 0, \quad \langle \xi_\alpha(t) \xi_\beta(t') \rangle = 2D \delta_{\alpha\beta} \delta(t - t'). \quad (5)$$

The fluctuation strength D will be determined empirically by comparing the resulting velocity variance with that obtained from single-vehicle data, see below. For low traffic densities, where the interactions can be neglected, Eq. (4) with (5) is an ordinary stochastic differential equation for v_α . In the stationary limit, it leads to the distribution function $w(v_\alpha) = (2\pi D\tau)^{-1} \exp[-(v_\alpha - V_0)^2/(2D\tau)]$. This means that, in the low-density limit of negligible interactions, the fluctuating strength D of the fluctuating forces (5) is related to the velocity variance $\theta = \langle (v_\alpha - V_0)^2 \rangle$ by $\theta = D\tau$ (fluctuation-dissipation relation). In Sec. II B, it will be shown that this relation holds for stationary traffic at all densities.

The equations (4) with (5) represent a microscopic traffic model on its own. It remains, however, to specify the ‘‘microscopic’’ braking interactions $\bar{f}_{\alpha\beta}$. In real traffic, these interactions depend in a complicated manner on the own velocity, and on the distances and velocities of the vehicles in front. To formulate reasonable assumptions for the GKT model, we will use averaged quantities like the density $\rho(x, t) = \int dv \tilde{\rho}(x, v, t)$, which is justified since we want to derive a macroscopic model. As a consequence, however, a simple purely microscopic equivalent of the GKT model exists only in some special cases.

Specifically, we make the following simplifying assumptions: i) A driver at position x reacts to the traffic situation at the advanced ‘‘interaction point’’

$$x_a = x + \gamma(l + Tv), \quad (6)$$

where $l = 1/\rho_{\max}$ (with maximum density ρ_{\max}) is the average vehicle length plus the bumper-to-bumper distance kept in standing traffic, and γ is an average anticipation factor with typical values between 1.0 and 3.0. In the limit of congested traffic, the interaction point is γ vehicle positions in front of the actual vehicle position x . Notice that, in the limit of congested traffic and for $\gamma = 1$, assumption i) corresponds to classical car-following models [30,10,28,13]. ii) In the light

of a mean-field ansatz, the traffic situation at the interaction point can be described by the density and the velocity distributions at this place, i.e., by the phase-space density $\tilde{\rho}(x_a, v, t)$. iii) There is a certain percentage $p(\rho_a) \equiv 1/\chi(\rho_a)$ of interaction-free space that allows drivers to approach the respective car in front before they brake. This percentage is a decreasing function of the average density $\rho_a = \int dv \tilde{\rho}(x_a, v, t)$ at the interaction point with $p(0) = 1$, and $p(\rho_{\max}) = 0$. It is determined by the condition that, in homogeneous dense traffic, the vehicles follow each other with a time headway of T . Furthermore, we assume that the probability of undelayed overtaking by lane changing is given by p as well [31]. Notice, that the factor $\chi = 1/p$ can be interpreted as the increase of the interaction rate due to the finite space requirements and positional correlations of vehicles, compared to point-like objects [18–20,28]. iv) If a driver is faster than the velocity v_a at the interaction point, and if he cannot overtake by lane changing [what happens with probability $(1 - p)$], he reduces his velocity abruptly to v_a as soon as the distance to the interaction point (moving with velocity v_a) has decreased by his share $\Delta x_{\text{free}} = p/\rho_a$ of the interaction-free space [32]. ($1/\rho_a$ is the average center-to-center distance between two vehicles at x_a).

Now, we formulate the kinetic equation underlying the GKT model. Taking the time derivative of the definition (1) of the phase-space density, and inserting the microscopic equations (2) and (4), gives, by partial integration, the kinetic evolution equation for the phase-space density [28],

$$\frac{\partial \tilde{\rho}}{\partial t} + \frac{\partial}{\partial x}(\tilde{\rho}v) + \frac{\partial}{\partial v} \left[\tilde{\rho} \frac{V_0 - v}{\tau} \right] = \frac{\partial}{\partial v}(\tilde{\rho}f_{\text{int}}) + \frac{\partial^2}{\partial v^2}(\tilde{\rho}D), \quad (7)$$

where the interaction term has the general form

$$f_{\text{int}} = \tilde{\rho}^{-1} \sum_{\alpha} \sum_{\beta (\neq \alpha)} \int dt' \int dx' \int dv' g(t - t', x - x', v - v') \times \bar{f}_{\alpha\beta} \delta[x' - x_\alpha(t)] \delta[v' - v_\alpha(t)]. \quad (8)$$

The four assumptions for the microscopic braking interactions $\bar{f}_{\alpha\beta}$ directly result in a Boltzmann-like interaction with a density-dependent prefactor $P(\rho)$:

$$\frac{\partial}{\partial v}(\tilde{\rho}f_{\text{int}}) = P(\rho)\mathcal{I}(x, v, t) \quad (9)$$

with

$$\begin{aligned} \mathcal{I}(x, v, t) = & \int_{v' > v} dv' (v' - v) \tilde{\rho}(x, v', t) \tilde{\rho}(x_a, v, t) \\ & - \int_{v' < v} dv' (v - v') \tilde{\rho}(x, v, t) \tilde{\rho}(x_a, v', t). \end{aligned} \quad (10)$$

The first term of (10) describes the increase of the phase-space density $\tilde{\rho}(x, v, t)$ due to the deceleration of faster

vehicles with velocity $v' > v$ which cannot overtake vehicles at x_a driving with velocity v , whereas the second term delineates the decrease of the phase-space density due to decelerations of vehicles driving with v which cannot overtake slower vehicles at x_a driving with $v' < v$. The prefactor

$$P(\rho) = (1-p)\chi = \frac{1}{p} - 1 \quad (11)$$

is proportional to the probability $(1-p)$ that one cannot immediately overtake a slower vehicle, and to the correlation factor $\chi = 1/p$ describing the increased interaction rate due to vehicular space requirements.

In summary, the kinetic phase-space equation upon which the GKT model is based, is given by

$$\begin{aligned} \frac{\partial \tilde{\rho}}{\partial t} + \frac{\partial}{\partial x}(\tilde{\rho}v) + \frac{\partial}{\partial v} \left[\tilde{\rho} \frac{V_0 - v}{\tau} \right] \\ = \left(\frac{1}{p} - 1 \right) \left[\int_{v' > v} dv' (v' - v) \tilde{\rho}(x, v', t) \tilde{\rho}(x_a, v, t) \right. \\ \left. - \int_{v' < v} dv' (v - v') \tilde{\rho}(x, v, t) \tilde{\rho}(x_a, v', t) \right] \\ + \frac{\partial^2}{\partial v^2}(\tilde{\rho}D). \end{aligned} \quad (12)$$

For $\gamma = 1$ and for dense traffic, the underlying microscopic dynamics is that of a microscopic, stochastic car-following model. In this case, traffic behaves like a one-dimensional gas of inelastic hard “vehicular molecules” with anisotropic interactions whose effective sizes vary with the local density such that there is a space $\Delta x_{\text{free}}(\rho_a)$ between the molecules.

B. Derivation of the Basic Equations

Following the standard procedure summarized in Refs. [28,18], we derive from the kinetic equation (12) macroscopic equations for the lowest velocity moments. In particular, we are interested in the dynamics of the macroscopic vehicle density $\rho(x, t)$ per lane and the average velocity $V(x, t)$ defined by

$$\rho(x, t) = \int_0^\infty dv \tilde{\rho}(x, v, t), \quad (13)$$

$$V(x, t) \equiv \langle v \rangle = \rho^{-1} \int_0^\infty dv v \tilde{\rho}(x, v, t). \quad (14)$$

As usual, one obtains an infinite hierarchy of equations where that for the n th moment depends on the $(n+1)$ st moment. In particular, the macroscopic density equation depends on V , and the macroscopic equation for V on the variance

$$\theta(x, t) \equiv \langle (v - V)^2 \rangle = \rho^{-1} \int dv (v - V)^2 \tilde{\rho}(x, v, t). \quad (15)$$

In the GKT model, we close the hierarchy by two assumptions. First, we assume that the variance θ is a function of density and average velocity. Second, we assume that the phase-space density is locally associated with a Gaussian velocity distribution

$$\tilde{\rho}(x, v, t) = \rho(x, t) \frac{e^{-[v - V(x, t)]^2 / [2\theta(x, t)]}}{\sqrt{2\pi\theta(x, t)}}. \quad (16)$$

This is well compatible with empirical velocity distributions obtained from single-vehicle data [28,33], at least, if the percentage of trucks is negligible [34]. Ansatz (16) is also consistent with the fluctuating force (5) in the microscopic Eq. (4). A more general ansatz taking into account small deviations from local equilibrium can be found in [22].

Multiplying the phase-space equation (12) with 1 or v , respectively, and integrating over v leads, after straightforward but lengthy calculations, to

$$\frac{\partial \rho}{\partial t} + \frac{\partial(\rho V)}{\partial x} = 0, \quad (17)$$

$$\begin{aligned} \left(\frac{\partial}{\partial t} + V \frac{\partial}{\partial x} \right) V = -\frac{1}{\rho} \frac{\partial(\rho\theta)}{\partial x} + \frac{V_0 - V}{\tau} \\ - \frac{P(\rho_a)\rho_a(\theta + \theta_a)}{2} B(\delta_V), \end{aligned} \quad (18)$$

where we used the notation $f_a(x, t) \equiv f(x_a, t)$ with $f \in \{\rho, V, \theta\}$. It turned out, that the approximation of the sum $(\theta + \theta_a)/2 \approx \theta$ leads only to negligible quantitative changes [35]. On the other hand, the approximation simplifies the velocity equation considerably, so we will adopt it henceforth. The monotonically increasing macroscopic interaction term

$$B(\delta_V) = 2 \left[\delta_V \frac{e^{-\delta_V^2/2}}{\sqrt{2\pi}} + (1 + \delta_V^2) \int_{-\infty}^{\delta_V} dy \frac{e^{-y^2/2}}{\sqrt{2\pi}} \right] \quad (19)$$

describes the dependence of the braking interaction on the dimensionless velocity difference $\delta_V = (V - V_a)/\sqrt{\theta + \theta_a}$. For $\gamma = 1$, the macroscopic interaction term can be easily understood by the underlying microscopic dynamics of the GKT model. If a vehicle at location x with velocity v is faster than one at x_a with velocity v_a (i.e. $\delta v = v - v_a > 0$), it approaches the car in front within the time $\Delta t = \Delta x_{\text{free}}/\delta v$, where $\Delta x_{\text{free}} = p/\rho_a$ is the average interaction-free distance $\Delta x_{\text{free}} = p/\rho_a$ of a car. Then, if it cannot overtake immediately, which would happen with probability $(1-p)$, it abruptly reduces the velocity by δv . The resulting ensemble-averaged deceleration is

$$\langle \delta v / \Delta t \rangle = -\frac{(1-p)}{p} \rho_a \int_0^\infty d(\delta v) (\delta v)^2 w(\delta v). \quad (20)$$

If v and v_a are uncorrelated and Gaussian distributed [cf. Eq. (16)], with expectation values V , V_a and variances θ , θ_a , respectively, the distribution function $w(\delta v)$ of the velocity difference is also a Gaussian, with expectation value $V - V_a = \sqrt{\theta + \theta_a} \delta v$ and variance $(\theta + \theta_a)$. Evaluating integral (20) yields $\langle \delta v / \Delta t \rangle = -\frac{1}{2} P \rho_a (\theta + \theta_a) B(\delta v)$, i.e., the macroscopic braking term in Eq. (18).

The assumption of a Gaussian velocity distribution alone would close the system after the variance equation, which can also be derived from the kinetic equation (12) [22,23]. Since a dynamic variance equation is not necessary for the description of known traffic instabilities, we close the system already after the velocity equation and assume for the variance the local equilibrium value $\theta = D\tau$ of the variance equation [22,23]. Notice that this relation for the variance is the same relation as derived in Sec. II A for low densities.

To complete the derivation of the GKT equations, we have to specify the ‘‘constitutive relation’’ for the quasi-adiabatically eliminated variance as a function of ρ and V , and the relation for the dimensionless correlation prefactor $P(\rho)$. The empirical data suggest that the variance (and thus D) is a density-dependent fraction $A(\rho)$ of the squared velocity,

$$\theta = A(\rho)V^2, \quad (21)$$

and that the variance prefactor A is higher in congested traffic than in free traffic. For qualitative considerations, A can be chosen to be constant. In the following, however, we approximate the empirical data by the Fermi function

$$A(\rho) = A_0 + \Delta A \left[\tanh \left(\frac{\rho - \rho_c}{\Delta \rho} \right) + 1 \right], \quad (22)$$

where A_0 and $A_0 + 2\Delta A$ are about the variance prefactors for free and congested traffic, respectively, ρ_c is of the order of the critical density for the transition from free to congested traffic, and $\Delta \rho$ denotes the width of the transition.

Now, we determine the correlation function $P(\rho)$ by imposing that the time headways in dense, homogeneous traffic are given by T . Solving Eq. (18) for stationary and homogeneous traffic of density ρ leads to the equilibrium velocity-density relation

$$V_e(\rho) = \frac{\tilde{V}^2}{2V_0} \left(-1 \pm \sqrt{1 + \frac{4V_0^2}{\tilde{V}^2}} \right) \quad (23)$$

with

$$\tilde{V} = \sqrt{\frac{V_0}{\tau \rho A(\rho) P(\rho)}}. \quad (24)$$

This also determines the equilibrium traffic flow per lane by

$$Q_e(\rho) = \rho V_e(\rho). \quad (25)$$

In the limit of high-densities, $(1 - \rho/\rho_{\max}) \ll 1$ (or $V_e \ll V_0$), this reduces to $V_e = \tilde{V}$. On the other hand, time headways of T and average gaps of $s = (1/\rho - 1/\rho_{\max})$ between the vehicles correspond to a velocity $V_T(\rho) = s/T = (1/\rho - 1/\rho_{\max})/T$. Demanding $V_e = V_T$ for high densities leads to

$$P(\rho) = \frac{V_0 \rho T^2}{\tau A(\rho_{\max})(1 - \rho/\rho_{\max})^2}. \quad (26)$$

This expression is consistent also in the other limit of homogeneous traffic with very low density. With Eq. (26), the macroscopic braking term $-P\rho\theta$ of Eq. (18) for homogeneous traffic is proportional to ρ^2 , in accordance with intuition: The rate of encountering a slower vehicle is proportional to ρ . Furthermore, the probability that one cannot overtake immediately by lane-changing when a slower vehicle is encountered, is proportional to ρ as well, resulting in a proportionality to ρ^2 at low densities. The interpretation of $p = (P + 1)^{-1}$ as the percentage $\rho \Delta x_{\text{free}}$ of free space is also consistent for both limiting cases. For $\rho \rightarrow \rho_{\max}$, one has $\Delta x_{\text{free}} \rightarrow 0$. For $\rho/\rho_{\max} \ll 1$, one obtains $\Delta x_{\text{free}} - \Delta x = V_0 T^2 / (\tau A_0)$. This means, vehicles on a nearly empty road would react to other vehicles in front (mostly by lane-changing), if these vehicles were closer than $V_0 T^2 / (\tau A_0)$. This is the net safety distance $V_0 T$ times a factor $T / (A_0 \tau)$ that is of order unity (see Table I).

C. Discussion of the Model

For convenience, let us summarize the equations of the GKT model. The traffic density and average velocity evolve, in absence of on- and off-ramps according to

$$\frac{\partial \rho}{\partial t} + \frac{\partial(\rho V)}{\partial x} = 0, \quad (27)$$

$$\left(\frac{\partial}{\partial t} + V \frac{\partial}{\partial x} \right) V = -\frac{1}{\rho} \frac{\partial(\rho A V^2)}{\partial x} + \frac{V_0 - V}{\tau} - \frac{V_0 A(\rho)}{\tau A(\rho_{\max})} \left(\frac{\rho_a T V}{1 - \rho_a / \rho_{\max}} \right)^2 B(\delta v), \quad (28)$$

where $B(\delta v)$ is given by Eq. (19). (For a generalization to cases with on- and off-ramps see Ref. [26].) $A(\rho)$ is the measured or assumed variance in units of the squared velocity, for which we use relation (22) throughout this paper.

The density equation (27) is just a one-dimensional continuity equation reflecting the conservation of the number of vehicles. Thus, the temporal change $\partial \rho / \partial t$ of the vehicle density is just given by the negative gradient $-\partial Q / \partial x$ of the lane-averaged traffic flow $Q = \rho V$.

The first term on the rhs of Eq. (28) is the gradient of the ‘‘traffic pressure’’ $\rho\theta = \rho A V^2$. It describes the kinematic dispersion of the macroscopic velocity in inhomogeneous traffic as a consequence of the finite velocity

variance. For example, the macroscopic velocity in front of a small vehicle cluster will increase *even if no individual vehicle accelerates*, because the faster cars will leave the cluster behind. The kinematic dispersion also leads to a smooth density profile at the dissolution front between congested traffic and an empty road, as it occurs when a road blockage at x_0 is removed at a time t_0 . In this case, the first vehicles can all accelerate to their respective desired velocities. Thus, after sufficiently long times, the high-speed tail of the distribution of desired velocities translates into a distribution of vehicle positions.

The second term of Eq. (28) denotes the acceleration towards the (traffic-independent) average desired velocity V_0 of the drivers with a relaxation time τ . Individual variations of the desired velocity are accounted for by the finite velocity variance.

The third term of Eq. (28) models braking in response to the traffic situation at the advanced “interaction point” $x_a = x + \gamma(1/\rho_{\max} + TV)$. The braking deceleration increases coulomb-like with decreasing gap $(1/\rho_a - 1/\rho_{\max})$ to the car in front ($1/\rho_a$ being the average distance between successive vehicle positions and $1/\rho_{\max}$ the minimum vehicle distance). In homogeneous dense traffic, the acceleration and braking terms compensate for each other at about the safe distance. In general, the deceleration tendency depends also on the velocity difference to the traffic at the interaction point, characterized by the “Boltzmann factor” $B(\delta_V)$. In homogeneous traffic, we have $B(0) = 1$. In the limiting case $\delta_V \gg 0$ (where the preceding cars are much slower), it follows $B(\delta_V) = 2\delta_V^2$. If, in contrast, the preceding cars are much faster (i.e. $\delta_V \ll 0$), we have $B(\delta_V) \approx 0$. That is, since the distance is increasing, then, the vehicle will not brake, even if its headway is smaller than the safe distance.

The main difference with respect to other macroscopic traffic models is the non-local character of the braking term, which we obtained by derivation from realistic assumptions of driving behavior. The non-locality has very favorable properties with respect to the robustness of numerical integration methods and their integration speed. It has smoothing properties like the viscosity term used in the Kerner-Konhäuser model [3,5], but its effect is anisotropic. There is no smoothing in forward direction, which would imply that cars would react on density or velocity gradients of the vehicles behind them.

The GKT model fits into the general class of macroscopic traffic models [18,28] defined by the continuity equation (27) and the velocity equation

$$\left(\frac{\partial}{\partial t} + V \frac{\partial}{\partial x} \right) V = -\frac{1}{\rho} \frac{\partial \mathcal{P}}{\partial x} + \frac{1}{\tau} [\tilde{V}_e(\rho, V, \rho_a, V_a) - V]. \quad (29)$$

In the GKT model, the “traffic pressure” \mathcal{P} is given by

$$\mathcal{P} = \rho\theta = \rho A(\rho)V^2, \quad (30)$$

and the “dynamical equilibrium velocity”, towards which the average velocity relaxes in the actual traffic situation, is

$$\tilde{V}_e(\rho, V, \rho_a, V_a) = V_0 \left[1 - \frac{A(\rho)}{2A(\rho_{\max})} \left(\frac{\rho_a TV}{1 - \rho_a/\rho_{\max}} \right)^2 B(\delta_V) \right]. \quad (31)$$

In contrast to other macroscopic models [36,16,3] belonging to the class defined by Eq. (29), the “dynamical equilibrium velocity” depends on ρ and V at *two* different locations, thus introducing the non-locality.

The five parameters of the GKT model, listed in Table I, are all intuitive. Three of them, V_0 , T , and ρ_{\max} , can be directly determined by fitting the equilibrium flow density relation (25) of the GKT model to measured flow-density data, cf. Fig. 1. The desired velocity V_0 is determined by fitting the data at low densities by a straight line $Q(\rho) = V_0\rho$. The safe time headway T and the maximum density ρ_{\max} are determined by fitting the data at high densities by a straight line crossing the abscissa at ρ_{\max} and identifying this line with $Q(\rho) = (1 - \rho/\rho_{\max})/T$. The ensuing average distance $1/\rho_{\max}$ of two cars in standing traffic must be consistent with the average length of the vehicles plus a minimal bumper-to bumper distance kept, which is about 1.5 m. As real traffic is stable at very low and very high densities, the above procedure of comparing the measured data in these density ranges with the *equilibrium* curve of the GKT model is justified. At intermediate densities, the equilibrium curve of the model lies somewhat above the data (Fig. 1). However, in Sec. III it will be shown that homogeneous traffic is unstable in this density range, and that the averaged *dynamic* traffic flow in the GKT model is below the equilibrium curve as well.

The remaining parameters τ and γ can be systematically calibrated by means of the dynamic properties. This will be discussed in Sec. IV. Table I lists the numerical values resulting from a fit to traffic data of the Dutch motorway A9. If not stated otherwise, we used these values in the numerical simulations of Sec. III, referring to them as “standard parameter set”.

Notice that all parameters have realistic values. In particular, this holds for τ which, for $V_0 = 158$ km/h, would have the meaning of the acceleration time from 0 to 100 km/h. Furthermore, V_0/τ is limited to the average maximum acceleration of vehicles on a free road starting with zero velocity. For these reasons, a relaxation time $\tau \approx 35$ s is sensible for freeway traffic. (For city traffic, τ is shorter).

The value $T = 1.8$ s for the safe time headway is consistent with the rule “distance (in m) should not be less than half the velocity (in km/h)” suggested by German authorities. For other data, however, we often find that a somewhat smaller time headway gives a better fit.

Since the model parameters are meaningful, it is simple to model changes of the traffic dynamics caused by

external effects like environmental influences. For example, a speed limit would be considered by decreasing V_0 . Bad weather conditions leading to more defensive driving would be characterized by an increased time headway T and a lower value of V_0 (plus a reduction of γ , if there is heavy fog). In rush-hour traffic, it is plausible to assume a higher percentage of experienced drivers than in holiday traffic, which would correspond to a higher γ . Effects like a varying distribution of vehicle types can be modelled as well. For example, a higher proportion of trucks would lead to a decrease of V_0 and ρ_{\max} , but also to an increased value of τ .

Finally, we compare the macroscopic GKT model with direct simulations of microscopic models of the form (4). While the microscopic model is stochastic, the deterministic GKT model includes the stochasticity of real traffic by the constitutive relation (21) for the velocity variance. Therefore, the GKT describes *macroscopic* effects of fluctuations like kinematic dispersion. The additional information of individual fluctuations contained in microscopic models seems not to be of practical relevance, since empirical traffic data are typically available as one-minute averages, i.e. in terms of macroscopic quantities.

In contrast to microscopic models, the GKT model is an effectively one-lane model and treats overtaking and the associated lane-changing manoeuvres in an overall way. A microscopic model would need additional assumptions and new parameters for the lane-changing decisions as well as additional assumptions about the population of vehicles, e.g., the distribution of desired velocities. Moreover, the macroscopic model can be generalized to simulate on-ramps, off-ramps, and lane closings, simply by adding source and sink terms to the macroscopic density and velocity equations (27) and (28) [25,26]. In microscopic models this would require the treatment of lane changes from dead-end lanes, which is a particularly difficult problem.

Finally, apart from very low densities, the numeric performance of simulations with the GKT model is far superior to corresponding microscopic simulations. This is achieved partly by using lookup tables for the functions $A(\rho)$ and $B(\delta_V)$ and by applying explicit integration schemes [37]. In addition, the GKT model has only one density and velocity field variable, and its computational speed (measured in terms of the length of the road sections that can be simulated real-time) is independent of the density and the number of lanes.

D. Dimensionless Form of the GKT Equations

By reformulating the GKT model in dimensionless variables, the number of model parameters can be reduced by two. We measure times in units of τ and distances in units of $1/\rho_{\max}$ by introducing $t' = t/\tau$ and $x' = \rho_{\max}x$. The dependent variables $\rho' = \rho/\rho_{\max}$, $V' = V\tau\rho_{\max}$, $\theta' = \theta\tau^2\rho_{\max}^2$, etc. are scaled accordingly.

This leads to the scaled GKT equations

$$\frac{\partial \rho'}{\partial t'} + \frac{\partial(\rho'V')}{\partial x'} = 0 \quad (32)$$

and

$$\left(\frac{\partial}{\partial t'} + V' \frac{\partial}{\partial x'} \right) V' = -\frac{1}{\rho'} \frac{\partial}{\partial x'} (\rho' \theta') + (V'_0 - V') - P' A'(\rho') \frac{(\rho'_a V')^2}{(1 - \rho'_a)^2} B(\delta_V), \quad (33)$$

where

$$A'(\rho') = \frac{A(\rho_{\max}\rho')}{A(\rho_{\max})} \quad (34)$$

is of order unity, and the Boltzmann term $B(\delta_V)$ (i.e., Eq. (19) in scaled variables), remains unchanged. The remaining dimensionless parameters are the scaled desired velocity

$$V'_0 = \rho_{\max}\tau V_0 \quad (35)$$

and the scaled cross-section

$$P' = \frac{\rho_{\max}V_0 T^2}{\tau} = V'_0 \left(\frac{T}{\tau} \right)^2, \quad (36)$$

in addition to the anticipation factor γ from the unscaled equations.

The parameter V'_0 , with a numerical value of 171.4 for the standard parameter set, has some analogies to the Reynolds number in the Navier–Stokes equations for normal fluids. Assuming that typical velocities are proportional to the desired velocities, typical densities proportional to ρ_{\max} , and typical length scales proportional to $1/\rho_{\max}$, this can be seen by observing that the magnitude of the destabilizing advection, pressure, and braking terms in the unscaled velocity equation (28) is proportional to $\rho_{\max}V_0^2$, while the stabilizing relaxation term is proportional to V_0/τ . So, the ratio between the destabilizing “kinetic” terms and the stabilizing relaxation term is proportional to $\rho_{\max}V_0\tau = V'_0$. As will be shown in Sec. III B, homogeneous traffic can become unstable, if a certain “critical” value V'_c is exceeded.

The scaled cross-section P' , with a numerical value of 0.453 for the standard parameter set, gives the ratio between the interaction term and the “kinetic” advection and pressure terms. In analogy to the Prandtl number of thermal convection in a simple fluid heated from below [38], it depends on the ratio of the two relevant time scales T and τ of the system.

As in the unscaled equations, the parameter γ characterizes the sensitivity in the braking interactions to spatial changes of the velocity, compared to the sensitivity for changes of the density.

III. RESULTS

A. Homogeneous Traffic

In homogeneous and stationary traffic, the GKT equations (27) and (28) reduce to $\rho = \text{const.}$ and relation (23) for the equilibrium velocity $V_e(\rho)$. Notice that $V_e(\rho)$ and thus the equilibrium flow $Q_e = \rho V_e(\rho)$ is a function of the model parameters V_0 , T , and ρ_{\max} , but does not depend on τ and γ .

We determined the constants in the relation (22) for the variance prefactor $A(\rho)$ and the model parameters V_0 , T , and ρ_{\max} , by fitting them to empirical data of the Dutch two-lane motorway A9 from Haarlem to Amsterdam. The empirical data are based on one-minute values for the number n_t of passing vehicles, their average velocity V_t , and velocity variance θ_t , which were determined from single-vehicle data. The corresponding flow is then given by $Q_t = n_t/2$ per minute and lane, and the density per lane by Q_t/V_t . Such sets of one-minute values were sampled over two periods from Monday to Friday (October 10, 1994 through October 14, 1994 and October 31, 1994 through November 4, 1994) for the right and left lane at nine subsequent measuring cross-sections (distributed over a stretch of 8.6 km length; see Ref. [39] for an illustration). To obtain empirical quantities as a function of density, we averaged over all sets with a density between $\rho - \Delta\rho$ and $\rho + \Delta\rho$ with $\Delta\rho = 1$ vehicle/km.

Figure 1(a) shows the variance prefactor Eq. (22) for the fitted values

$$\begin{aligned} \rho_c &= 0.27\rho_{\max}, \\ \Delta\rho &= 0.05\rho_{\max}, \\ A_0 &= 0.008, \text{ and} \\ \Delta A &= 2.5A_0. \end{aligned} \quad (37)$$

Throughout the paper, we will use these values.

Figure 1(b) depicts the flow-density relation for the fitted values of V_0 , T , and ρ_{\max} given in Table I. These values resulted from the systematic procedure described in Sec. III D. Both the empirical variance-density relation and the flow-density relation are well reproduced by introducing *one* fit function $A(\rho)$ only. With a constant value for A , the sharp increase of the variance prefactor at a density of about 40 vehicles/km and the sharp decrease of the velocity related to it could not be obtained by variation of V_0 , T , and ρ_{\max} . Rather, this correlation is an intrinsic property of the model and follows from the proportionality of the braking interaction to the variance. Notice, that the deviation of the assumed variance prefactor from the data at very low densities could be easily removed by a more complicated function $A(\rho)$. However, this correction would not impair the flow-density relation, because the interaction is negligible for these densities. For the same reason, the correction would not change the dynamics, justifying the choice of the simple functional dependence (22).

In the plots of Fig. 2, the resulting equilibrium flow $Q_e = \rho V_e(\rho)$ is plotted as a function of the density for various values of the model parameters V_0 , T , and ρ_{\max} . The solid lines in the plots 2(a) - 2(d) show the result for the standard parameter set of Table I.

Figures 2(a) and (b) illustrate that, according to our model, traffic flow will increase with growing desired velocity V_0 and with decreasing safe time headway T , as expected. The desired velocity V_0 mainly influences the low-density regime, while T is relevant for high densities. This is also underlined by Figs. 3(a) and 3(b), which show the equilibrium velocity for the same parameters. As expected, a reduction of V_0 (e.g. caused by a speed limit or an uphill gradient) influences traffic only at low densities. Since a reduction of V_0 increases the stability of homogeneous traffic (see below), this has practical implications. A variable speed limit, which is active only above a certain density threshold, would increase the stability without reducing the capacity of the road.

The changes of traffic flow resulting from variations of ρ_{\max} are plausible as well [Fig. 2(c)]. Decreasing ρ_{\max} or, equivalently, increasing the average vehicle length (corresponding to a higher percentage of trucks) reduces the maximum flow (capacity) of the road. Of course, a higher proportion of trucks also leads to a lower desired velocity. These combined effects are shown in Fig. 2(d).

B. Stability of Homogeneous Traffic With Respect to a Localized Perturbation

The homogeneous and stationary equilibrium solution (23) investigated in Sec. III A is not always stable. Here, we consider its stability with respect to a localized perturbation in the initial conditions. Specifically, we assume a dipole-like initial variation of the average density $\bar{\rho}$ according to

$$\begin{aligned} \rho(x, 0) &= \bar{\rho} + \Delta\rho \left[\cosh^{-2} \left(\frac{x - x_0}{w^+} \right) \right. \\ &\quad \left. - \frac{w^+}{w^-} \cosh^{-2} \left(\frac{x - x_0 - \Delta x_0}{w^-} \right) \right], \end{aligned} \quad (38)$$

as suggested in Ref. [40]. The positive and negative peaks are positioned at x_0 and $x_0 + \Delta x_0$, respectively, with $\Delta x_0 = 1006.25$ m, and they have the widths $w^+ = 201.25$ m, and $w^- = 805$ m, respectively. The amplitude $\Delta\rho$ of the perturbation will be varied in the simulations. The initial flow $Q(x, 0) = Q_e(\rho(x, 0))$ is assumed to be in local equilibrium everywhere. Our simulations showed that the specific shape of the perturbation is not relevant. Moreover, localized perturbations of a different form (e.g., a constant density plus a Gaussian perturbation of the average velocity) were, after a short time, transformed to dipole-like perturbations similar to that of Eq. (38). The simulations were carried out with explicit finite-difference methods [41].

Figure 4 shows the spatio-temporal evolution of the initial perturbation (38) with $\Delta\rho = 10$ vehicles/km for various initial densities $\bar{\rho}$. In Fig. 4(a), it is shown that the perturbation dissipates, if the traffic density is sufficiently low. When increasing the initial density, perturbations eventually lead to instabilities. Depending on the density, a single density cluster [cf. Fig. 4(b)], or a cascade of traffic jams (i.e., stop-and-go traffic) [Fig. 4(c)] is triggered. If one further increases the density, we observed dipole-like structures similarly to those described in Ref. [24]. Finally, for densities above 50-55 vehicles/km, one reaches again a stable regime [Fig. 4(d)].

The underlying instability mechanism is intuitive [5]. In the perturbation (38), the positive density peak (with a lower velocity than in the homogeneous regions) is behind the negative peak (with higher velocity). This means, drivers in the region upstream of the perturbation will approach the positive peak. If the traffic density is sufficiently low, the vehicles can overtake by lane changing without braking, as soon as they meet the tail of the perturbation. In addition, the perturbation dissolves by the above described effect of kinematic dispersion. As a result, homogeneous traffic is stable at low densities. For higher densities, however, a higher percentage of drivers approaching the density peak must brake, thereby locally increasing the density. The increased density, in turn, gives a positive feedback for further braking reactions. This feedback cycle continues until the resulting velocity is so low that the acceleration term compensates the braking effects. This defines the jammed density $\rho = \rho_{\text{jam}}$ with nonzero flow $Q = Q_e(\rho_{\text{jam}})$. Furthermore, it makes plausible that homogeneous traffic of density $\bar{\rho} \geq \rho_{\text{jam}}$ is stable again.

An important criterium for realistic traffic models is, that the transition to these inhomogeneous states should be hysteretic, corresponding to a first-order phase transition [5]. This implies that, at least in some parameter range, the response of the system to localized perturbation depends on the perturbation amplitude (bistability). In terms of real traffic, there are situations where traffic flow is metastable with respect to small perturbations, but it breaks down if the perturbations are sufficiently large. Figure 5 shows that we found two ranges of densities, $\bar{\rho} \in [\rho_{c1}, \rho_{c2}]$ and $\bar{\rho} \in [\rho_{c3}, \rho_{c4}]$, where the transition is bistable. For large perturbation amplitudes, the system develops to a localized-cluster state if $\bar{\rho} \in [\rho_{c1}, \rho_{c2}]$, or to a dipole-like state if $\bar{\rho} \in [\rho_{c3}, \rho_{c4}]$, while it relaxes back to the equilibrium state for smaller perturbations. Between these ranges, there is a region $\bar{\rho} \in [\rho_{c2}, \rho_{c3}]$, where homogeneous traffic is linearly unstable, giving rise to cascades of density clusters (“stop-and-go waves”). For $\rho < \rho_{c1}$ and $\rho > \rho_{c4}$, traffic is stable for arbitrary perturbations.

In Fig. 5(a), we plot the minimum and maximum densities ρ_{min} and ρ_{jam} that resulted from simulations of traffic on a circular road after a dynamic steady state has been reached. A large difference ($\rho_{\text{jam}} - \rho_{\text{min}}$) corresponds to localized-cluster or stop-and-go states, while

($\rho_{\text{jam}} - \rho_{\text{min}}$) ≈ 0 is the signature of the homogeneous state. At a perturbation amplitude of one vehicle per km (dashed lines), the perturbation can be considered as being linear, while at $\Delta\rho = 20$ vehicles/km (dotted lines), the perturbation amplitude reaches the order of the homogeneous densities defining the maximum perturbation. So, we can determine from the plot the four critical densities. Notice that the densities ρ_{jam} and ρ_{min} of the developed non-linear state depend neither on the initial density nor on the amplitude of the perturbation. Figure 6 shows the basins of attraction of the two traffic states in the phase space spanned by $\bar{\rho}$ and $\Delta\rho$. For values of ($\bar{\rho}, \Delta\rho$) corresponding to points inside the two curves, the final steady-state consists of density clusters or stop-and-go waves. Otherwise, the final state is that of homogeneous equilibrium.

Now, we will show that the stability of the model is determined mainly by the relaxation time τ and by the anticipation factor γ . Since the flow-density relation does not depend on these parameters, this means that one can calibrate the stability and the flow rates independently. Figures 5(b) and 6 show that an increased value of τ leads both to an increased range of instability, and to increased amplitudes ($\rho_{\text{jam}} - \rho_{\text{min}}$) of the non-linear state. If τ exceeds values of about 60 s, the density exceeds the maximum density ρ_{max} in the course of the simulations, which is a signature of accidents. For $\tau \leq 12$ s, the unstable and metastable regions vanish altogether, and the system is globally stable for all densities and all perturbation amplitudes. For a fixed value $\gamma = 1.2$ but otherwise arbitrary model parameters, global stability is reached, if the dimensionless parameter $V'_0 = \rho_{\text{max}} V_0 \tau$ of the scaled equations (32) and (33) satisfies $V'_0 \leq V'_c = 59$. Further simulations showed that the stability of traffic described by the GKT model increases also with increasing γ . Both the critical relaxation time where accidents occur, and the critical value V'_c for global stability increase. This is plausible since γ describes the anticipation of future velocity changes.

It turned out that the qualitative difference between the non-linear state of Fig. 4(b), where only one cluster is seen, and that of Fig. 4(c), where a cascade of stop-and-go waves appeared, can be understood by the linearly unstable and metastable density ranges discussed above. In both cases, there is a region in the wake of the first cluster, where the density is lower, and the velocity is higher than in the homogeneous region downstream. This gives rise to a transition layer between these regions serving as a small perturbation [5]. In Fig. 4(b), the system is metastable, and this perturbation is too small to induce a new density cluster. In Fig. 4(c), the system is linearly unstable and the transition layer triggers a new cluster. This cluster, in turn, gives rise to a new transition layer eventually leading to a cascade of stop-and-go waves.

Another remarkable feature of Fig. 4(c) is that the width of the first (upstream) stop-and-go wave is growing while the other waves remain narrow. The width of

the cluster in Fig. 4(b) increases as well, but slower. This can be explained by observing that the growth rate of the width is given by the difference of the group velocities $v_{g,\text{up}} = (Q_{\text{jam}} - Q_{\text{in}})/(\rho_{\text{jam}} - \rho_{\text{in}})$ and $v_g = (Q_{\text{out}} - Q_{\text{jam}})/(\rho_{\text{out}} - \rho_{\text{jam}})$ of the upstream and downstream fronts (Fig. 7). For the density $\bar{\rho} = 25$ vehicles/km corresponding to Fig. 4(b), the difference is small, while for $\bar{\rho} = 35$ vehicles/km [Fig. 4(c)], it is large. In all subsequent clusters of Fig. 4(c), we have $Q_{\text{in}} = Q_{\text{out}}$ and $\rho_{\text{in}} = \rho_{\text{out}}$, so they do not grow.

It is required for any realistic traffic model, that the density ρ_{jam} inside localized clusters and the traffic in the region downstream of it is independent of the inflow [5]. This implies that the group velocity v_g should be constant. The upper curves in Fig. 5 for the jam density, the dashed line of Fig. 7 for v_g , and the dashed line of Fig. 8 for Q_{out} show, that the GKT model essentially fulfills this requirement.

Another frequently discussed problem is, to which extent equilibrium flow-density relations of traffic models can be calibrated by non-equilibrium empirical data. In Fig. 9 we simulate the measurement of traffic data by recording the velocity and density at several fixed locations (“measuring cross-sections”) over a certain period of time. To incorporate the distribution of densities encountered in real traffic, we run simulations for various densities. In each run, the simulation time was proportional to the occurrence probability of traffic densities in the course of the day, for which we assumed a linear decrease from a maximum value at $\bar{\rho} = 0$ to zero for $\bar{\rho} = 70$ vehicles/km. The dots in Figure 9 show the flows and densities “measured” at the cross-sections for all simulation runs put together. In addition, the solid line in Fig. 8 shows the dynamic average of the flow for runs at a given density. Both figures show that, in the case of unstable traffic, the flow of the “measured” dynamic flow-density relation (broken line) is considerably lower than the equilibrium flow. From this it follows that, in regions of unstable traffic, one cannot calibrate equilibrium flows of traffic models to empirical flow-density relations.

C. Fronts Between Congested and Free Traffic

The realistic description of shock fronts in traffic is a particularly difficult problem, as pointed out in Ref. [42]. Therefore, in this section we will investigate how fronts between two different states of traffic, especially between free and congested traffic, evolve in the GKT model. We model such fronts by initial conditions containing discontinuities in the fields ρ and V . In particular, we consider shocks at x_{shock} between two homogeneous regions with densities ρ_1 and ρ_2 at the left (upstream) and right (downstream) sides. Initial conditions with $\rho_1 > \rho_2$ include situations of dissolving jams. The extreme case $\rho_1 = \rho_{\text{max}}$ corresponds to vehicles starting from standstill after a road blockage is removed. Initial conditions

with $\rho_1 < \rho_2$ include situations, where free traffic flow meets a queue of nearly standing vehicles. The simulations were carried out with the standard parameter set of Table I. At the upstream boundary ($x = 0$ km), we chose the fixed (Dirichlet) boundary conditions $\rho(0, t) = \rho_1$ and $Q(0, t) = Q_e(\rho_1)$ to model a constant inflow consistent with the initial conditions. At the downstream boundary ($x_{\text{max}} = 40$ km), we simulated an unperturbed outflow by the homogeneous von Neumann conditions $\partial_x \rho(x_{\text{max}}, t) = \partial_x Q(x_{\text{max}}, t) = 0$. Figure 10(a) and 10(b) show the spatio-temporal development of the density and the flow for $\rho_1 < \rho_2$ (upstream jam-fronts).

One can see that the shape of the backwards moving front does not change in time [cf. Fig.10(a)] and that there is no region of negative velocity [Fig.10(b)]. This is achieved by the non-local interaction term in the velocity equation, while a viscosity term ($\sim \partial^2 V / \partial x^2$) would make the front smoother with increasing time.

Figures 11(a) and 11(b) show the spatio-temporal evolution of the density and flow for downstream fronts with $\rho_1 \gg \rho_2$. This corresponds to a dissolving jam (for example, after an accident has been cleared) with an outflow to a nearly empty road section. Due to the kinematic dispersion term $(1/\rho)\partial(\rho\theta)/\partial x$ in the velocity equation, the forward moving front is somewhat smoothed in the course of time. The finite velocity variance implies that, after some time, the faster cars are found in a wider distance from the jam front.

As a remarkable fact it should be mentioned that, although the equilibrium point of the outflow ($\rho_{\text{out}}, Q_e(\rho_{\text{out}})$) is the result of a dynamic process, the outflow Q_{out} is nearly constant over a wide range of ρ_1 [cf. Fig.12(a)]. This agrees with empirical observations where it has been found that the outflow of very different forms of congested traffic (including the dissolution of queued city traffic after a traffic light turns green) is nearly a “constant of traffic” [8,43].

This generalizes the above mentioned requirement of a constant outflow from clusters (whose jam density is determined by the dynamics) to forms of congestion that are a result of the initial and boundary conditions.

However, the outflow Q_{out} varies with the model parameters. It increases with growing γ [cf. Fig.12(b)], because an acceleration tendency is already recognized in a larger distance from the jam front. The outflow decreases drastically with increasing T [cf. Fig.12(c)], because T determines the time headway between two following vehicles or, equivalently, the inverse of the flow. Furthermore, the outflow is diminished with increased τ [cf. Fig.12(d)], because increased values of τ correspond to lower accelerations and thus to more inert vehicles.

D. Method of Parameter Calibration

While the model parameters V_0 , T , and ρ_{max} influence the equilibrium flow-density (or velocity-density) relation

(Figs. 2 and 3), the parameters τ (Fig. 5) and γ influence only the stability behavior. This enables an effective calibration of the GKT model to concrete traffic situations.

First, V_0 is determined as the low-density limit of the experimental velocity-density relation (which, in this limit, is also the equilibrium relation), and ρ_{\max} is determined by the average length of the vehicles and assuming a reasonable bumper-to bumper distance of, e.g., 1.5 m in standing traffic. Then, T is calibrated by the observed maximum flows, by the outflows from stop-and-go waves, or by the flow resulting from standing traffic after a red light turns green or an obstacle is removed [8,43]. Afterwards, one calibrates τ and γ by the observed stability behavior (Fig. 5) and by the shape and width of the downstream and upstream fronts connecting free and congested states (Figs. 10 and 11).

Since τ and γ weakly influence the flows [Figs. 12(d) and 12(b)], the calibration of T , τ , and γ is repeated recursively until convergence is obtained.

Applying this procedure to the single-vehicle data of the Dutch motorway A9 leads to the parameter set shown in Table I. Notice that, because of their immediate intuitive meaning, the plausible range of values for the model parameters is rather restricted. One can argue that reasonable time headways are in the range $T \in [1.0\text{s}, 2.5\text{s}]$, and that initial accelerations $a_{\max} = V_0/\tau$ are in the range $a_{\max} \in [1 \text{ m/s}^2, 4 \text{ m/s}^2]$ corresponding (e.g. for $V_0 = 144 \text{ km/h}$) to $\tau \in [10\text{s}, 40\text{s}]$. Finally, the minimum anticipation of traffic is to the car in front, implying $\gamma \geq 1$.

IV. SUMMARY AND CONCLUSIONS

We have proposed a macroscopic gas-kinetic-based traffic model (GKT model) that was derived from a microscopic model of vehicle dynamics. The assumed fluctuations of vehicle acceleration implied a velocity distribution of finite variance which is governed by a kinetic equation related to that used in kinetic gas theory. In the resulting GKT equations, the velocity variance enters both the braking interactions and the smoothing effect of the “kinematic dispersion”.

In contrast to gas-kinetic-based models proposed earlier [18,21], we could now derive the correlation factor reflecting the increased interaction rate of vehicles at high densities by simple and plausible arguments. Furthermore, we replaced the dynamic variance by a “constitutive relation” obtained from single-vehicle data, thereby considerably simplifying the description. The resulting relation of the flow as a function of the density agreed well with empirical data. Since the form of this function is determined by the constitutive relation, this supports the assumption of the model that braking interactions are mainly caused by a finite velocity variance.

Because of its derivation from physical assumptions, all model parameters of the GKT model have an intuitive meaning and can be either directly measured or cal-

ibrated to real traffic data. It is straightforward to model the effects of, e.g., speed limits, varying road conditions (e.g., gradients), or different driving behavior. Moreover, we proposed a systematic calibration procedure.

In contrast to other macroscopic traffic models, the GKT model is non-local. While the non-locality has similar smoothing effects as a diffusion or viscosity term, it leads to a more favourable numerical stability behavior. The model belongs to the class of effective one-lane models, so multi-lane aspects are treated only in a global way. Nevertheless, it is straightforward to include ramps [26], or lane blockages (e.g., due to road works or accidents).

Investigations of instabilities arising from a localized perturbation of homogeneous traffic showed qualitatively the same scenario as has been found for the model of Kerner and Konhäuser [5,24]. For sufficiently high values of τ , homogeneous traffic at intermediate densities becomes unstable with respect to perturbations, leading to non-linear states like localized clusters, stop-and-go waves, or dipole-like structures, while homogeneous traffic flow is stable for high and low densities. The GKT model satisfies two requirements which should hold for any realistic model [5]. First, the transition to localized clusters is hysteretic. Second, the outflow region of the clusters is nearly independent of the homogeneous density. In contrast to most other models, however, the traffic flow within the clusters is finite and can be influenced by the model parameters τ and γ . This enables the simulation of “synchronized” traffic states [26] that turned out to be the most frequent form of congested traffic [1].

Only for high densities and for $\gamma = 1$, the interaction term of the microscopic equations (4) underlying the GKT model can be written in terms of a simple car-following model. For this case, we performed simulations with a smoothed version of Eq. (4) (containing no abrupt velocity changes in the interaction term) and found a nearly quantitative agreement in describing collective states like clusters or stop-and go waves.

The high numerical stability of the GKT model also allowed to treat realistic boundary conditions (instead of the periodic boundary conditions used in most previous publications), and to simulate discontinuous fronts between homogeneous low-density and high-density states. Such fronts correspond to the formation or dissolution of jammed traffic that is caused by initial or boundary conditions rather than by dynamic instabilities.

Remarkably, the outflow Q_{out} from jammed regions was nearly the same as the outflow from localized clusters, regardless of the density of the jams, including even standstill traffic (related, e.g., to the dissolution of a queue behind a traffic light turning green). The observation that the outflow from arbitrary kinds of congested traffic is a “universal” constant of traffic dynamics, and also its numerical value of about 1800 vehicles per hour, agrees well with observations of real traffic [8,43]. Besides the constant group velocity of localized clusters, this universal outflow can be considered as an additional requirement for realistic traffic models.

Acknowledgments

The authors want to thank for financial support by the BMBF (research project SANDY, grant No. 13N7092) and by the DFG (Heisenberg scholarship He 2789/1-1). They are also grateful to Henk Taale and the Dutch *Ministry of Transport, Public Works and Water Management* for supplying the freeway data.

-
- [1] B. S. Kerner and H. Rehborn, Phys. Rev. Lett. **49**, 4030 (1997).
- [2] D. Helbing and B. A. Huberman, Nature, in print (1998).
- [3] B. S. Kerner and P. Konhäuser, Phys. Rev. E **48**, R2335 (1993).
- [4] D. Helbing, Phys. Rev. E **51**, 3164 (1995).
- [5] B. S. Kerner and P. Konhäuser, Phys. Rev. E **50**, 54 (1994).
- [6] B. S. Kerner and H. Rehborn, Phys. Rev. E **53**, R4275 (1996).
- [7] B. S. Kerner and H. Rehborn, Phys. Rev. E **53**, R1297 (1996).
- [8] B. S. Kerner, in *Transportation Systems*, edited by M. Papageorgiou and A. Pouliezios (International Federation of Automatic Control, Chania, Greece), Vol. II.
- [9] D. Helbing, “Cellular automaton model simulating experimental properties of traffic flows”, submitted (1998).
- [10] M. Bando, K. Hasebe, K. Nakanishi, A. Nakayama, A. Shibata, and Y. Sugiyama, J. Phys. I France **5**, 1389 (1995).
- [11] B. Barlovic, L. Santen, A. Schadschneider, and M. Schreckenberg, in *Traffic and Granular Flow '97*, edited by M. Schreckenberg and D. Wolf (Springer, Singapore, 1998).
- [12] S. Krauß, *Microscopic Modelling of Traffic Flow: Investigation of Collision Free Vehicle Dynamics* (DLR, Cologne, 1998), FB 98-08.
- [13] D. Helbing and B. Tilch, Phys. Rev. E **58**, 133 (1998).
- [14] I. Prigogine and R. Herman, *Kinetic Theory of Vehicular Traffic* (Elsevier, New York, 1971).
- [15] S. L. Paveri-Fontana, Transportation Research **9**, 225 (1975).
- [16] W. F. Phillips, Transportation Planning and Technology **5**, 131 (1979).
- [17] D. Helbing, Phys. Rev. E **53**, 2366 (1996).
- [18] D. Helbing, Physica A **233**, 253 (1996).
- [19] C. Wagner *et al.*, Phys. Rev. E **54**, 5073 (1996).
- [20] A. Klar and R. Wegener, J. Stat. Phys. **87**, 91 (1997).
- [21] D. Helbing, Phys. Rev. E **57**, 6176 (1998).
- [22] D. Helbing and M. Treiber, Granular Matter **1**, 21 (1998).
- [23] D. Helbing, in *A Perspective Look at Nonlinear Media. From Physics to Biology and Social Sciences*, edited by J. Parisi, S. C. Müller, and W. Zimmermann (Springer, Berlin, 1998).
- [24] B. S. Kerner, P. Konhäuser, and M. Schilke, Physics Letters A **215**, 45 (1996).
- [25] B. S. Kerner, P. Konhäuser, and M. Schilke, Phys. Rev. E **51**, 6243 (1995).
- [26] D. Helbing and M. Treiber, Phys. Rev. Lett., in print (1998); M. Treiber and D. Helbing, “Macroscopic simulation of widely scattered synchronized traffic states”, J. Phys. A: Math. Gen., submitted (1998).
- [27] Possible forms of the localized weighting function include $g(t-t', x-x', v-v') = f(t-t')f(x-x')f(v-v')$ with, e.g., $f(t-t') = \frac{1}{\Delta t} \Theta(|t-t'| - \frac{\Delta t}{2})$, or $f(t-t') = \frac{1}{\sqrt{2\pi}\Delta t} \exp\{(t-t')^2/[2(\Delta t)^2]\}$.
- [28] D. Helbing, *Verkehrsdynamik* (Springer, Berlin, 1997).
- [29] L. D. Landau and E. M. Lifshitz, *Fluid Mechanics* (Addison Wesley, Reading, MA, 1959).
- [30] D. C. Gazis, R. Herman, and R. W. Rothery, Operations Research **9**, 545 (1961).
- [31] This implicitly assumes a certain gap distribution and a certain aggressiveness in lane changing.
- [32] Notice that, in the case $\gamma > 1$, v_a is not the velocity of the car in front, but the coarse-grained velocity at a point x_a in front of the predecessor. A factor $\gamma > 1$ means that one anticipates future velocity changes of the car in front. Thus, γ is a measure of the experience and attentiveness of the drivers.
- [33] D. Helbing, Phys. Rev. E **55**, 3735 (1997).
- [34] Otherwise one would obtain a bimodal distribution where the two peaks would correspond to typical desired velocities of cars and trucks.
- [35] The approximation $(\theta + \theta_a)/2 \approx \theta_a$ leads to quantitative changes of dynamic properties of the order of 10%, but simplifies the velocity equation considerably. The simplification is justified in the dimensionless equations, because they are mainly used for fundamental investigations of instability properties and not for a quantitative comparison with empirical data.
- [36] H. J. Payne, in *Mathematical Models of Public Systems*, edited by G. A. Bekey (Simulation Council, La Jolla, CA, 1971), Vol. 1.
- [37] D. Helbing and M. Treiber, “Numerical simulation of macroscopic traffic models”, Computers in Physics, submitted (1998).
- [38] M. C. Cross and P. C. Hohenberg, Rev. Mod. Phys. **65**, 851 (1993).
- [39] D. Helbing, Phys. Rev. E **55**, R25 (1997).
- [40] M. Herrmann and B. S. Kerner, Physica A **255**, 163 (1998).
- [41] R. J. LeVeque, *Numerical Methods for Conservation Laws* (Birkhäuser, Basel, 1992).
- [42] C. F. Daganzo, Transportation Research B **29**, 277 (1995).
- [43] R. A. Raub and Pfefer, in *77th TRB Annual Meeting* (Transportation Research Board, Washington, D.C., 1998), manuscript no. 004.

Parameter	Symbol	Typical Value
Desired Velocity	V_0	110 km/h
Maximum Density	ρ_{\max}	160 vehicles/km
Acceleration Relaxation Time	τ	35 s
Time Headway	T	1.8 s
Anticipation Factor	γ	1.2

TABLE I. Typical parameter values of the GKT model used for the simulations throughout this paper. The values were obtained by calibration of the model parameters to Dutch freeway data.

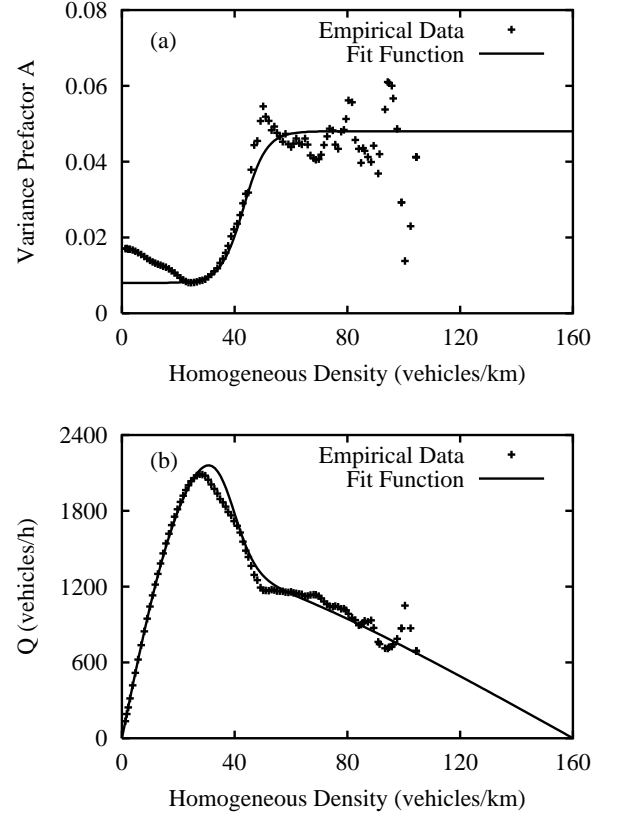
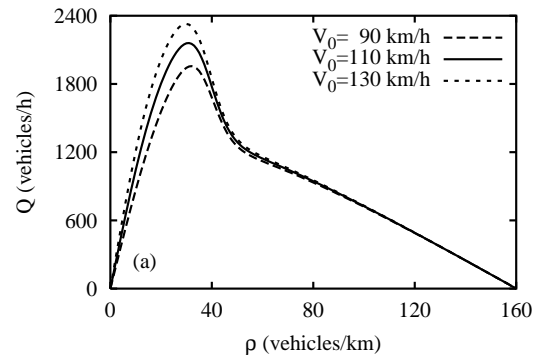


FIG. 1. Comparison of (a) the density-dependent relative variance in units of the squared average velocity, and (b) the equilibrium flow-density relation (25) in the GKT model (solid lines) with empirical data (crosses). The empirical data were obtained from single-vehicle data of the Dutch motorway A9 by averaging over one-minute intervals (see main text).



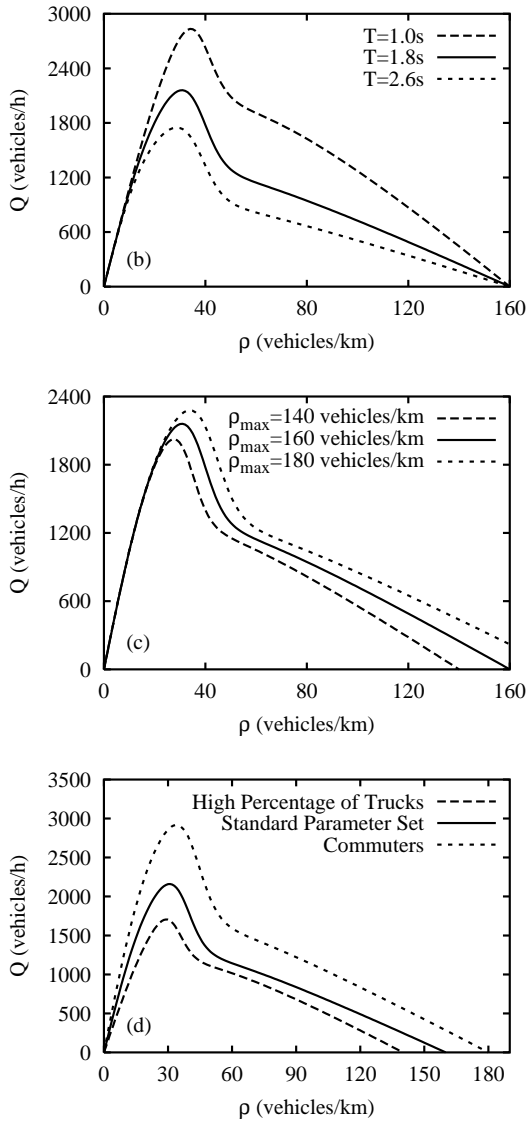


FIG. 2. Equilibrium flow-density relations of the GKT model. The diagrams (a) through (c) show the variation with the model parameters V_0 , T , and ρ_{\max} . In each diagram, the solid lines correspond to the standard parameter set displayed in Table I. Diagram (d) shows parameter combinations as one would expect for, e.g., an increased percentage of trucks ($V_0 = 80$ km/h, $T = 1.8$ s, $\rho_{\max} = 140$ vehicles/km), or a decreased percentage ($V_0 = 140$ km/h, $T = 1.4$ s, $\rho_{\max} = 180$ vehicles/km).

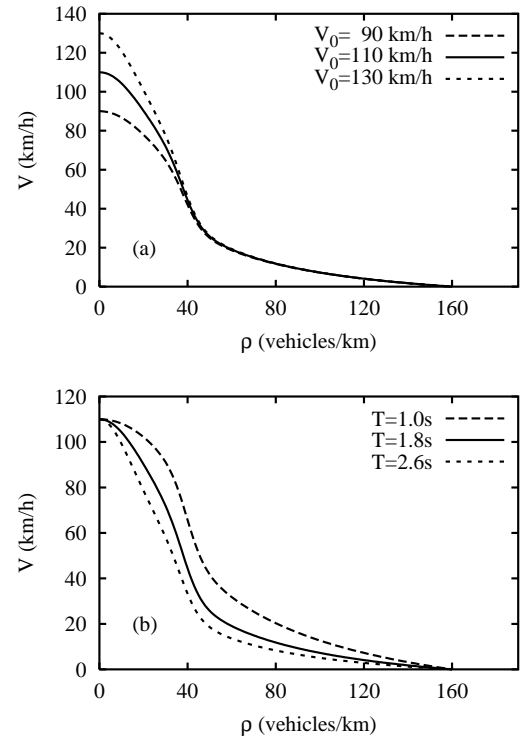
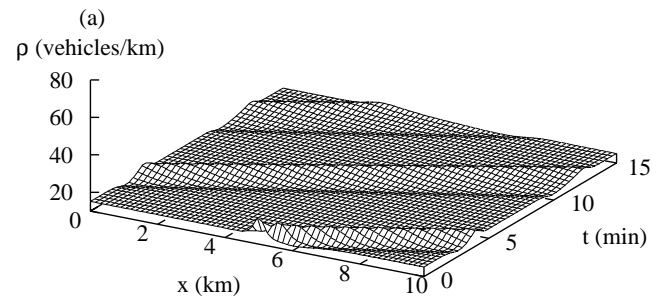


FIG. 3. Variation of the equilibrium velocity-density relation of the GKT model with (a) the desired velocity V_0 , and (b) the safe time headway T . The other parameters have the standard values displayed in Table I.



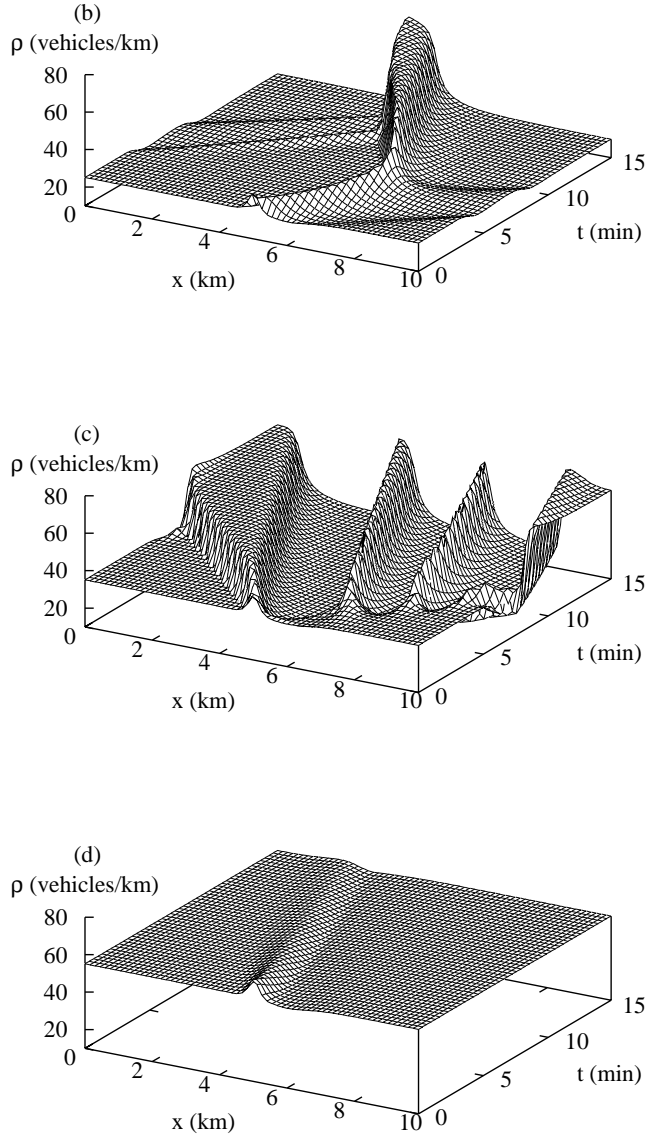


FIG. 4. Spatio-temporal evolution of traffic on a uni-directional ring of circumference 10 km, starting with initially homogeneous traffic (of density $\bar{\rho}$) to which a localized perturbation of amplitude $\Delta\rho = 10$ vehicles/km is added in accordance with Eq. (38). (a) is for $\bar{\rho} = 15$ vehicles/km (linearly stable), (b) and (c) are for unstable traffic ($\bar{\rho} = 25$ vehicles/km and 35 vehicles/km), and (d) is for stable congested traffic (55 vehicles/km). The model parameters are given by the standard set displayed in Table I.

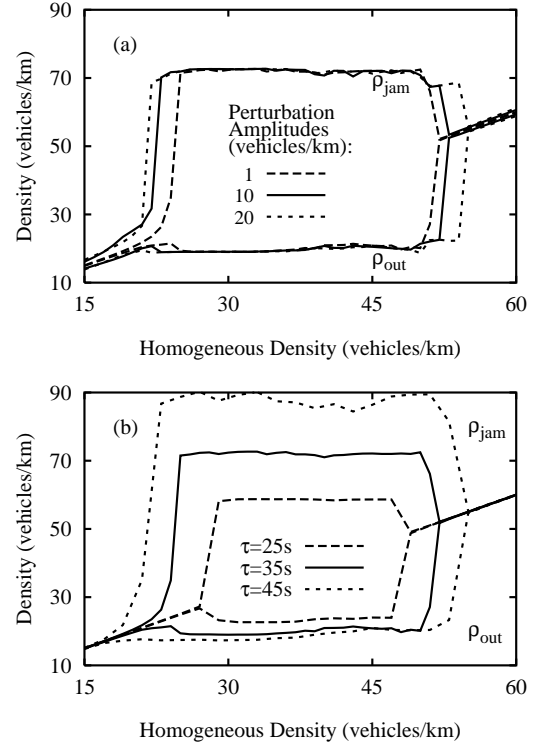


FIG. 5. Stability diagram for perturbations of homogeneous traffic of the form (38) in a ring of circumference 10 km. Both diagrams show the maximum and minimum densities ρ_{jam} and ρ_{out} as a function of the average density $\bar{\rho}$, measured after a dynamical equilibrium was reached. The unstable traffic regime corresponds to the density range where the jam amplitude ($\rho_{jam} - \rho_{out}$) is large (rectangle-like shaped regions). Diagram (a) shows the dependence of the stability diagram on the perturbation amplitude $\Delta\rho$. One can clearly see two density ranges $[\rho_{c1}, \rho_{c2}]$ with $\rho_{c1} = 21$ vehicles/km and $\rho_{c2} = 24$ vehicles/km, and $[\rho_{c3}, \rho_{c4}]$ with $\rho_{c3} = 51$ vehicles/km and $\rho_{c4} = 55$ vehicles/km, where traffic is non-linearly stable, i.e., stable for small perturbations, but unstable for large perturbations. In the range $[\rho_{c2}, \rho_{c3}]$, homogeneous traffic is unstable for arbitrary perturbation amplitudes. Diagram (b) shows the stability diagram for various relaxation times τ and a perturbation amplitude of $\Delta\rho = 1$ vehicle/km.

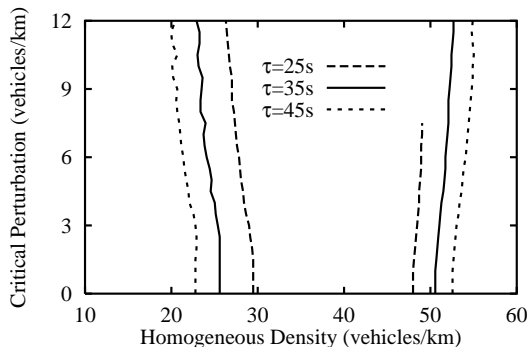


FIG. 6. Critical perturbation amplitudes $\Delta\rho_c$ of localized perturbations in the metastable (non-linearly unstable) density regime for various values of τ . The critical amplitude is the minimal amplitude that can cause traffic jam formation. Smaller amplitudes are damped out in the course of time. Between the two metastable density regions arbitrarily small perturbation amplitudes will cause the formation of traffic jams. At low and high densities, inhomogeneities of traffic flow tend to disappear.

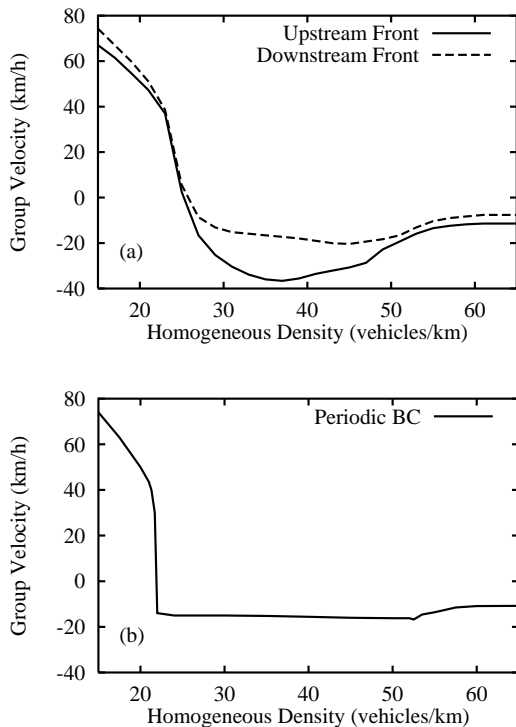


FIG. 7. (a) Group velocity of the upstream front (solid) and downstream front (dashed) of the first stop-and-go wave displayed in Fig. 4. The propagation of the fronts is calculated during a period, where the density of traffic jams does not grow anymore ($t > 4$ min), but the dynamics does not yet depend on the boundary conditions ($t < 15$ min). Notice that the propagation velocity at low densities is positive, but slower than the average vehicle velocity. In the instability region, the negative propagation velocity of the downstream front depends only weakly on the initial density, and its magnitude is well compatible with empirical data. The larger propagation velocity of the upstream front comes from the growing jam length. (b) Group velocity of the upstream and downstream fronts on a circular road. Here, the length of traffic jams stabilizes after some time, and their upstream fronts move with the same velocities as their downstream fronts. The magnitude of the initial perturbation ($\Delta\rho = 10$ vehicles/km) has been chosen larger than in diagram (a) ($\Delta\rho = 1$ vehicle/km), resulting in a larger region of negative group velocities.

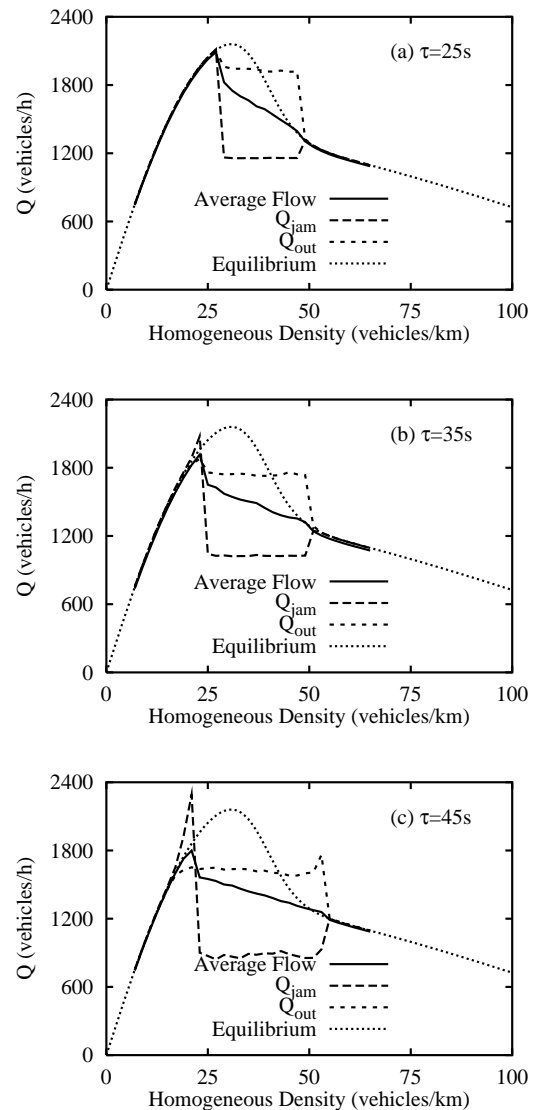


FIG. 8. Characteristic flows in the fully developed stop-and-go traffic corresponding to Fig. 5(b), which results on a circular road from locally perturbed traffic of average density $\bar{\rho}$. Depicted are, as a function of $\bar{\rho}$, the flows Q_{jam} in the jammed regions, the outflows Q_{out} from jams, and the average flows. For comparison, the equilibrium flow $Q_e = \rho V_e$ with V_e from Eq. (23) is also shown. Notice that, in the unstable range, the average *dynamic* flow is lower than the equilibrium flow.

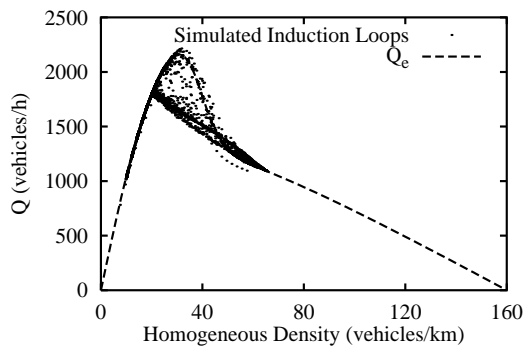


FIG. 9. Simulated flow-density relation as superposition of data obtained at five equally distributed “detectors” on a circular road of length 10 km (dots). In order to take into account the variation of traffic densities in the course of the day, the average density $\bar{\rho}$ was varied in the range [10 vehicles/km, 70 vehicles/km] in steps of 2 veh/km. The total duration of simulations for the homogeneous density $\bar{\rho}$ was $70 \text{ min} [1 - \bar{\rho}/(70 \text{ vehicles/km})]$. Note that, in the unstable regime, the dynamical flow-density values tend to lie below the equilibrium relation (dashed line).

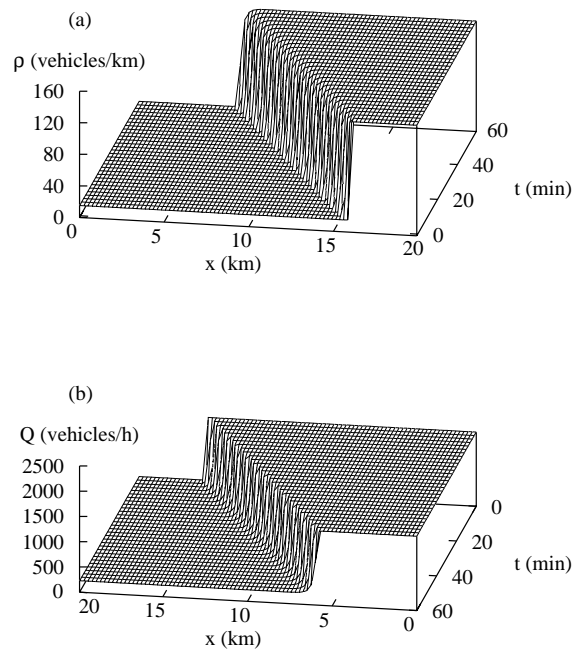


FIG. 10. Simulation of an upstream front with initial densities of $\rho_1 = 15 \text{ vehicles/km}$ and $\rho_2 = 140 \text{ vehicles/km}$. Shown is the spatio-temporal evolution of (a) the density, and (b) the flow. In (b), the direction of the space and time axes is reversed for illustrative reasons.

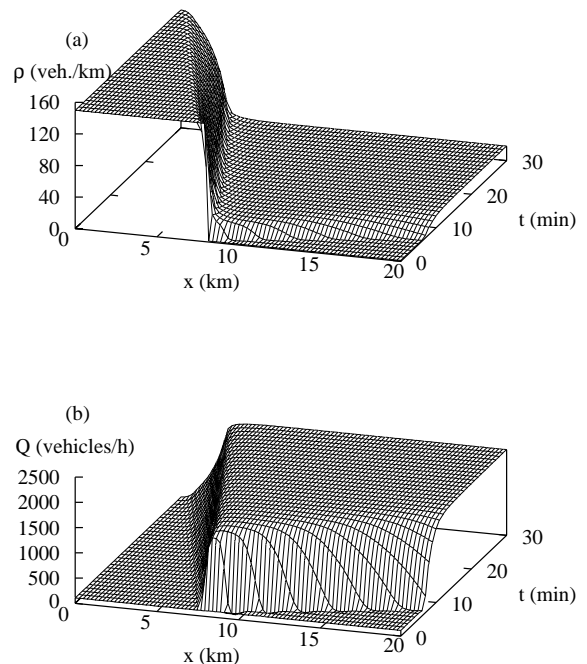


FIG. 11. Simulations of downstream-fronts with $\rho_{\text{jam}} = 140$ vehicles/km. Shown is the spatio-temporal development of (a) the density, and (b) the flow. Free boundary conditions were used on both sides.

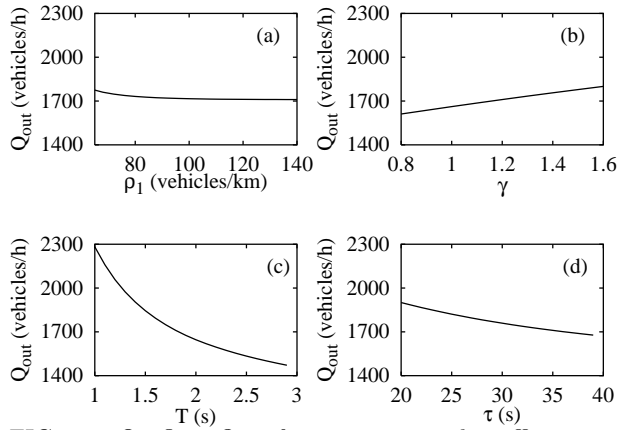


FIG. 12. Outflow Q_{out} from a congested traffic state of density ρ_1 in dependence of (a) ρ_1 , (b) γ , (c) T , and (d) τ . The simulated traffic situation is that of Fig. 11. The outflows were determined after a transient time of 30 minutes.

